



HAL
open science

Study of layered iron(III) phosphate phase $\text{Na}_3\text{Fe}_3(\text{PO}_4)_4$ used a positive electrode in lithium batteries

Khiem Trad, Dany Carlier-Larregaray, Alain Wattiaux, Mongi Ben Amara,
Claude Delmas

► **To cite this version:**

Khiem Trad, Dany Carlier-Larregaray, Alain Wattiaux, Mongi Ben Amara, Claude Delmas. Study of layered iron(III) phosphate phase $\text{Na}_3\text{Fe}_3(\text{PO}_4)_4$ used a positive electrode in lithium batteries. Journal of The Electrochemical Society, 2010, 157 (8), pp.A947-A952. 10.1149/1.3442365 . hal-00494474

HAL Id: hal-00494474

<https://hal.science/hal-00494474>

Submitted on 21 Oct 2010

HAL is a multi-disciplinary open access archive for the deposit and dissemination of scientific research documents, whether they are published or not. The documents may come from teaching and research institutions in France or abroad, or from public or private research centers.

L'archive ouverte pluridisciplinaire **HAL**, est destinée au dépôt et à la diffusion de documents scientifiques de niveau recherche, publiés ou non, émanant des établissements d'enseignement et de recherche français ou étrangers, des laboratoires publics ou privés.

Study of a layered iron(III) phosphate phase $\text{Na}_3\text{Fe}_3(\text{PO}_4)_4$ used as positive electrode in lithium batteries

Trad K., Carlier D., Wattiaux A., Ben Amara M., Delmas C.

Abstract : The layered $\text{Na}_3\text{Fe}_3(\text{PO}_4)_4$ phase prepared by solid-state reaction was studied as positive electrode in lithium batteries. Up to 1.9 Li^+ ions/f.u. could be intercalated, and only 1.7 Li^+ ions could be extracted between 4.5 and 2 V vs Li^+/Li with an average voltage of around ~ 2.8 V. In situ and ex situ X-ray diffraction data and Mössbauer spectroscopy measurements indicate that the intercalation/deintercalation process occurs through a solid solution process and is reversible. To improve its electrochemical performances, $\text{Na}_3\text{Fe}_3(\text{PO}_4)_4$ was also prepared via a hydrothermal method that leads to a significant particle size reduction. However, no clear improvements of the cycling performances were observed using this material as positive electrode in sodium and lithium batteries.

1. Introduction :

Recently, a new class of cathodic material based on iron phosphates gathered much attention for their high stability and economical and environmental interests. The strong inductive effect of the $(\text{PO}_4)^{3-}$ polyanion increases the potential of the transition-metal redox couple and then creates a relatively high operating potential for these $\text{Fe}^{\text{II}}/\text{Fe}^{\text{III}}$ compounds compared to oxides.¹ The $\text{Fe}^{3+}/\text{Fe}^{2+}$ redox voltage depends strongly on the crystal structure: For example, the discharge voltage in the Nasicon-type $\text{Li}_3\text{Fe}_2(\text{PO}_4)_3$ ² (2.8 V) is 0.7 V much lower than that in the olivine-type LiFePO_4 ,³ which lies at 3.5 V. Since the discovery of highly interesting electrochemical properties for LiFePO_4 , the search for novel polyanion-based insertion hosts is intense.^{4,5,6,7} Even some sodium-based phosphates were tested in lithium cells^{8,9,10,11} and exhibited interesting cycling performances. In this context, we were interested in a new sodium iron phosphate phase, $\text{Na}_3\text{Fe}_3(\text{PO}_4)_4$ recently reported by some of us.¹² $\text{Na}_3\text{Fe}_3(\text{PO}_4)_4$ exhibits a layered structure pretty similar to $\text{Na}_3\text{Cr}_3(\text{PO}_4)_4$ and $\text{K}_3\text{Fe}_3(\text{PO}_4)_4 \cdot \text{H}_2\text{O}$,^{13,14} with a complex framework built by layers of corner-sharing FeO_6 octahedra and PO_4 tetrahedra and Na^+ ions inserted between these layers. From a structural point of view, this structure can allow both ionic and electronic conductivities. In a previous paper, we reported the structural study [X-ray diffraction (XRD), Mössbauer, and NMR spectroscopies] of $\text{Na}_3\text{Fe}_3(\text{PO}_4)_4$ prepared as powder together with its behavior as positive electrode in sodium batteries:¹⁵ about 1.8 extra Na^+ ions could be reversibly intercalated within the 2.55–2 V potential range vs Na^+/Na with a low polarization (0.03 V at C/100 rate) of the cell. As the cycling performances in sodium cells were interesting, we also studied the electrochemical performances of $\text{Na}_3\text{Fe}_3(\text{PO}_4)_4$ used as positive electrode in lithium cells. In the present paper, we report the cycling properties, followed by the study (XRD and Mössbauer spectroscopy) of the evolution of the structure during the first electrochemical cycle. Finally, a tentative optimization of the electrochemical performance by reducing the particle size is given.

2. Experimental

The $\text{Na}_3\text{Fe}_3(\text{PO}_4)_4$ powder sample was synthesized through a solid-state reaction carried out in oxygen. Stoichiometric quantities of Na_2CO_3 , $\text{FeC}_2\text{O}_4 \cdot 2\text{H}_2\text{O}$, and $(\text{NH}_4)_2\text{H}_2\text{PO}_4$ were intimately mixed 2 h with a tridimensional mixer. This milling leads to the formation of $(\text{NH}_4)\text{FePO}_4 \cdot \text{H}_2\text{O}$ and Na_2CO_3 , which was then further milled during 1 h in a planetary mill using an agate vessel and agate balls. These precursors were thermal-treated under oxygen flow successively for 6 h at 400°C and 6 h at 600°C and annealed 3 days at 750°C with intermediate grinding between each thermal treatment. A light yellow powder was finally obtained by quenching the product in air. The stoichiometry of the mixture and the intimate mixing of the precursors had to be absolutely respected to get a pure phase. Otherwise, NaFeP_2O_7 and $\text{Na}_3\text{Fe}_2(\text{PO}_4)_3$ impurities were observed.

To improve the electrochemical performance by reducing the size particle, a hydrothermal synthesis was carried out. The precursors $\text{FePO}_4 \cdot 4\text{H}_2\text{O}$ (96%, Aldrich) and $\text{Na}_3\text{PO}_4 \cdot 12\text{H}_2\text{O}$ (98%, Aldrich) in a stoichiometric ratio were added to 25 mL distilled water mixed together and stirred for 10 min. The solution was transferred in a Teflon-lined Paar reactor and reacted at 200°C for 24 h. The final solution was cooled and filtered; the obtained precipitate was air-dried at 80°C overnight.

The particle morphology was characterized by scanning electron microscopy (SEM) using a field-emission microscope (Hitachi S-450).

XRD pattern was collected using a PANalytical X'Pert Pro diffractometer (Co $K\alpha$ radiation and iron filter, antiscatter slit of 0.5° and divergence slit of 1° on the incident beam path). The diffraction pattern was recorded in the 5–80° (2θ) angular range using a 0.0167° (2θ) step and a constant counting time of 10 s.

The cathode was made of 80% of active material, 15% of carbon black conductive additive, and 5% of polytetrafluoroethylene binder. The mixture was homogenized by ballmilling for 15 min then dried under vacuum at 100°C overnight. Into an argon-filled glove box, the mixture was finally crushed into a thin sheet and then was cut into a disk (14 mm diameter), and Swagelok-type cells were assembled. Metallic lithium was used as a negative electrode and a 1 M LiPF_6 solution in a mixture of propylene carbonate, ethylene carbonate, and dimethyl carbonate (DMC, 1:1:3) was used as an electrolyte. Two Celgard 2400 separators and a Viledon polypropylene foil were used as separators. The electrochemical tests were carried out in the galvanostatic mode with a homemade apparatus or with a Bio-logic VMP1 system. The open-circuit voltage (OCV) measurements consisted in 1 h discharge periods at a C/50 rate followed by open-circuit periods achieved when a 1 mV/h stability criteria is reached for the end of the relaxation period. For ex situ XRD analysis, the positive electrodes were removed from the cell in a dry box, washed with DMC, and dried under vacuum. For in situ XRD studies, a special cell was homemade with a Beryllium window. The diffraction patterns were recorded in operando at room temperature in the range 9–58° (2θ) in steps of 0.0167° (2θ) every 4 h ($\sim 0.04 \text{ Li}^+$ ions inserted).

Mössbauer spectroscopy has been used to study changes in oxidation state and iron coordination during the electrochemical cycling. Ex situ ^{57}Fe Mössbauer spectra were recorded on the electrode materials after the first discharge and charge. As the electrodes made at low potentials could be easily oxidized, they were handled with cautions and specific tied sample holders were used for analysis. The electrodes were sealed under argon atmosphere in a sample holder, which was transparent to the γ -rays. These measurements were performed at room temperature in transmission geometry with a constant acceleration spectrometer using ^{57}Co source in a Rh matrix equipped with a cryostat. The velocity was calibrated by using pure iron metal as a standard material at room temperature. All isomer shifts reported in this work refer to the natural α -Fe at 293 K. The spectra were fitted to Lorentzian profiles using the least-squares method. To ensure that our analysis was quantitative, it was necessary to evaluate the value of the Lamb–Mössbauer factor (f) (the recoil-free fraction of iron atoms that contributes to the Mössbauer effect) of each type of iron ions. Some measurements were therefore carried out at low temperature ($T=40.5 \text{ K}$) and confirmed that all Fe ion types have similar f factors.

3. Results and discussion

3.1. Structure

The XRD pattern of $\text{Na}_3\text{Fe}_3(\text{PO}_4)_4$ prepared as powder by solid-state reaction confirms that the phase is pure and well crystallized. As expected from results already obtained for single crystals, all the diffraction peaks of the XRD pattern could be indexed using the monoclinic $C2/c$ space group.¹² We performed the complete analysis of the XRD pattern by Rietveld refinement, taking into account size and strain effects as reported elsewhere.¹⁵ The cell parameters obtained for $\text{Na}_3\text{Fe}_3(\text{PO}_4)_4$ are $a=19.6494(3) \text{ \AA}$, $b=6.3924(1) \text{ \AA}$, $c=10.5969(2) \text{ \AA}$, and $\beta =91.776(1)^\circ$. The structure of $\text{Na}_3\text{Fe}_3(\text{PO}_4)_4$ is presented in Figure 1. It consists in layers parallel to the bc plane, formed by corner-sharing FeO_6 octahedra, which are further connected by phosphate tetrahedra through corner and edge sharing. The structure exhibits two different Fe sites [Fe(1) in 4d and Fe(2) in 8f] and two P (8f) sites, as shown in

Figure 1. Each Fe(1)O_6 octahedron has common corners with four Fe(2)O_6 octahedra and six PO_4 tetrahedra, whereas each Fe(2)O_6 octahedron has a common edge with a P(1)O_4 tetrahedron and shares corners with four other PO_4 tetrahedra and two Fe(1)O_6 octahedra. The sodium ions are located in the interslab space in two different fully occupied crystallographic sites [Na(1) in 4e and Na(2) in 8f]. Sodium ions in the Na(1) site have a six-coordinated oxygen environment with an axial symmetry, whereas sodium ions in Na(2) have a seven-coordinated oxygen environment. For further details on the local environment of the cations in this structure, please refer to [Ref. 15](#).

In this framework, the layers are not compact, and the structure exhibits tunnels along the $[110]$ and $[\bar{1}\bar{1}0]$ directions, as shown in [Figure 1\(c\)](#) (directions indicated in [Figure 1\(b\)](#)). These tunnels can provide an extra direction for alkaline ion diffusion; one can therefore expect a three-dimensional diffusion process.

SEM of $\text{Na}_3\text{Fe}_3(\text{PO}_4)_4$ sample prepared by solid-state reaction reveal that the aggregate sizes are around $6 \mu\text{m}$ and that the primary particles have an anisotropic platelet shape with diameters in the $0.8\text{--}1.5 \mu\text{m}$ range and thicknesses in the $0.2\text{--}0.4 \mu\text{m}$ range. The SEM characterization is shown below in comparison with the ones of the particles prepared by the hydrothermal route.

3.1. Electrochemical properties

Na^+/Li^+ ion exchange was first tested to try to get a new phase $\text{Li}_3\text{Fe}_3(\text{PO}_4)_4$ that could be tested in lithium cells. Several exchange conditions were used: LiCl and LiOH aqueous solutions (at different temperatures and pH values), LiCl solution in ethanol, and LiNO_3 molten salt but they always led to a decomposition of the initial phase into other known phosphates as $\text{FePO}_4 \cdot 2\text{H}_2\text{O}$, $\text{LiFePO}_4 \cdot \text{OH}$, or $\text{Li}_3\text{Fe}_2(\text{PO}_4)_3$. We therefore studied $\text{Na}_3\text{Fe}_3(\text{PO}_4)_4$, itself as positive electrode in lithium batteries. To check the stability of $\text{Na}_3\text{Fe}_3(\text{PO}_4)_4$ in the electrolyte, the powder was immersed for several hours, then washed with DMC and dried under vacuum. XRD and Mössbauer spectroscopy confirmed that there is no chemical reaction with the electrolyte used.

The galvanostatic cycling and OCV curves obtained for $\text{Na}_3\text{Fe}_3(\text{PO}_4)_4$ prepared by solid-state reaction used as positive electrode in a lithium cell are shown in [Figure 2](#). Up to 1.9 Li^+ ions/f.u. could be intercalated and only 1.7 Li^+ ions could be extracted between 2 and 4.5 V vs Li^+/Li ([Figure 2\(a\)](#)) with an average voltage of around $\sim 2.8 \text{ V}$ that is much lower than the one observed for the olivine LiFePO_4 ($\sim 3.5 \text{ V}$)³ for a same redox couple $\text{Fe}^{\text{III}}/\text{Fe}^{\text{II}}$. The discharge curve begins with a direct voltage drop to 2.65 V vs Li^+/Li followed by a flat voltage profile that spreads over a long range of lithium composition up to 1.0 Li^+ and then gradually slopes to 2 V. The OCV discharge curve is shown in [Figure 2\(b\)](#). No clear voltage plateau on a long range of lithium composition is observed but rather a gradual decrease in the voltage during Li^+ intercalation. However, based on these experiments, one cannot exclude that a voltage plateau is present on a very narrow lithium composition range at the beginning of the discharge. During the second cycle, similar discharge and charge profiles were observed, indicating a good reversibility of the cycling process. One could have expected a different cycling curve for the second cycle if Na^+ ions were deintercalated during the first charge instead of Li^+ ions. It seems not to be the case here.

For comparison, the cycling curve obtained with $\text{Na}_3\text{Fe}_3(\text{PO}_4)_4$ used as a positive electrode in a sodium cell is shown in [Figure 3](#). The shapes of the cycling curves are rather similar. Moreover, the sodium cell exhibits a low polarization of around 0.03 V for a C/100 cycling rate, indicating rather good ionic and electronic conductivities of the electrode, whereas the lithium cell exhibits a higher polarization for the same cycling rate. Because the electronic conductivities of the electrodes of both Na and Li cells are expected to be similar, we can assume that the electrode materials in lithium batteries exhibit a rather poor ionic conductivity. The capacities achieved in sodium and lithium batteries are small (around 80 mAh/g), but improvements are expected through optimization of the electrodes. In the last part of the paper, the cycling performances obtained for $\text{Na}_3\text{Fe}_3(\text{PO}_4)_4$ prepared by hydrothermal synthesis that exhibits smaller particles size are presented.

3.2. Ex situ and in situ XRD studies

Ex situ and in situ XRD techniques were used to study the crystal structure changes in $\text{Na}_3\text{Fe}_3(\text{PO}_4)_4$ during the discharge/charge cycle. [Figure 4\(a\)](#) shows the XRD patterns performed on the initial material and on the electrode

materials recovered at 1.5 V after the first discharge ($\text{Li}_{1.9}\text{Na}_3\text{Fe}_3(\text{PO}_4)_4$) and at 4.5 V at the end of the first cycle (it was not possible to remove all Li^+ ions during the first charge up to 4.5 V, so that the initial $\text{Na}_3\text{Fe}_3(\text{PO}_4)_4$ stoichiometry is not exactly recovered). Figure 4(b) shows the in situ XRD measurements performed on the electrode during the first discharge. All the peaks can be indexed in the $C2/c$ space group of $\text{Na}_3\text{Fe}_3(\text{PO}_4)_4$ indicating that the framework is maintained during the cycling process. Both ex situ and in situ experiments reveal that, contrarily to intercalation of Na^+ ions,¹⁵ the intercalation of Li^+ ions does not lead to a significant shift of the Bragg peaks but to a strong line broadening (Figure 4(a)4(b)). Moreover, this peak broadening is not symmetric as seen, for example, for the (200) and (110) peaks evolution during the first discharge recorded in situ (Figure 4(b)): The (200) line gets broader on the higher 2θ values side, whereas the (110) line gets broader on the lower 2θ values side. Such asymmetric peak broadening, observed for different diffraction lines, could be due to the formation of some structural distortion during the intercalation of the Li^+ ions. Note that, like for Na^+ ions intercalation, the nature of the sites occupied by the intercalated Li^+ ions have not yet been determined.

The XRD pattern of the electrode recovered at the end of the cycle recorded ex situ (Figure 4(a)) exhibits narrower diffraction peaks than the ones observed in $\text{Li}_{1.9}\text{Na}_3\text{Fe}_3(\text{PO}_4)_4$, indicating that the distortion created during Li^+ ion intercalation and Fe(III) ions reduction partially disappears while Li^+ are removed and Fe(II) ions are oxidized back.

3.3. Mössbauer spectroscopy

^{57}Fe Mössbauer spectroscopy was used to study the oxidation states and sites of iron ions involved in the electrochemical process during the first cycle. All the spectra were recorded in a large range of velocities (-10 and $+10$ mm/s) and show the absence of magnetic impurities in the samples and especially $\alpha\text{-Fe}_2\text{O}_3$, which is magnetic at room temperature.

The Mössbauer spectrum of $\text{Na}_3\text{Fe}_3(\text{PO}_4)_4$ exhibits two doublets (Figure 5(a)) attributed to the two different crystallographic Fe(III) sites based on their occupation ratio [$\text{Fe}(1)/\text{Fe}(2)\sim 0.5$]. The fitted parameters (Table I) indicate that the iron ions are trivalent with a high spin configuration and are located in octahedral environments as expected from the structure.¹⁵ The local environments of Fe(1) and Fe(2) in $\text{Na}_3\text{Fe}_3(\text{PO}_4)_4$ are shown in Figure 6.

At the end of the first discharge (1.5 V), 1.9 Li^+ ions were electrochemically intercalated and the Mössbauer spectra reveals the presence of two extra signals (Figure 5(b)) attributed to two high-spin-Fe(II) in octahedral sites in agreement with the reduction of some Fe(III) to Fe(II) during the intercalation of Li^+ ions. However, the total amount of Fe(II) observed ($\sim 46\%$) in $\text{Li}_{1.9}\text{Na}_3\text{Fe}_3(\text{PO}_4)_4$ is lower than that of the expected one ($\sim 63\%$). The origin of this difference is still unclear. We attributed the $\text{Fe}^{2+}(1)$ site to the 4d site and the $\text{Fe}^{2+}(2)$ site to the 8f site (see Table I) to keep the total occupation ratio of each site close to the initial values [$\text{Fe}(1)/\text{Fe}(2)=0.5$]. During the first discharge of the cell, it appears here that the Fe(III) ions in Fe(1) and Fe(2) sites are equivalently reduced because both ratios, the $\text{Fe}^{3+}(1)/\text{Fe}^{3+}(2)$ and $\text{Fe}^{2+}(1)/\text{Fe}^{2+}(2)$ ratios, are close to 0.5. In the sodium cell, we showed by Mössbauer spectroscopy that the $\text{Fe}^{3+}(2)$ ions were preferentially reduced during the first discharge indicating that the extra Na^+ ions are located somewhat closer to this iron site.¹⁵ This difference in behavior suggests different intercalation processes in both systems. Moreover, the fitted parameters of the two Fe(II) sites in $\text{Li}_{1.9}\text{Na}_3\text{Fe}_3(\text{PO}_4)_4$ are really different than those obtained for the spectra of $\text{Na}_{4.6}\text{Fe}_3(\text{PO}_4)_4$ given in Ref. 15. Therefore, the intercalated lithium ions should occupy different sites than the extra Na^+ ions in the structure. The Mössbauer spectra of the electrode at the end of the cycle (Figure 5(c)) is really similar to that of the starting material (Figure 5(a)) with only a little amount of Fe(II) remaining, thus confirming the good reversibility of the cycling process and in agreement with the fact that all the Li^+ ions could not be deintercalated up to 4.5 V. Based on these results, together with the shape of the cycling curve and the XRD ex situ patterns, only Li^+ ions are deintercalated from $\text{Li}_{1.9}\text{Na}_3\text{Fe}_3(\text{PO}_4)_4$.

3.3. Effect of the particle size

The powder morphology for a positive electrode material is important because a smaller grain size favors the intercalation process in the particles by reducing the ion-diffusion path length. We tried, thus, to decrease the particles size by preparing the $\text{Na}_3\text{Fe}_3(\text{PO}_4)_4$ phase by a hydrothermal route. Figure 7 shows the XRD pattern that

confirms the formation of $\text{Na}_3\text{Fe}_3(\text{PO}_4)_4$. A small amount of an impurity phase $\text{Na}_3\text{Fe}_2(\text{PO}_4)_3$ was detected (indicated by narrows on Figure 7). As seen in Figure 7, the diffraction lines of the phase prepared by hydrothermal reaction are broader than that of the phase obtained by solid-state reaction. Thermal analysis, performed on a Perkin-Elmer TGA, confirmed that the sample was not hydrated. The particles and aggregates sizes were analyzed by SEM. Figure 8 shows the SEM images of $\text{Na}_3\text{Fe}_3(\text{PO}_4)_4$ prepared by (a) hydrothermal reaction and (b) solid-state reaction. $\text{Na}_3\text{Fe}_3(\text{PO}_4)_4$ prepared by hydrothermal reaction consists in spherical aggregates of around 20 μm (Figure 8(a)) of very thin platelets, which ranges between 300 and 600 nm in their largest dimension and between 40 and 100 nm in thickness. Whereas, the aggregates are bigger than those of $\text{Na}_3\text{Fe}_3(\text{PO}_4)_4$ prepared by solid-state reaction, the particle size is much smaller (solid-state reaction: 1–1.5 μm in diameter and 200–400 nm in thickness). We therefore expected better electrochemical properties for $\text{Na}_3\text{Fe}_3(\text{PO}_4)_4$ prepared by the hydrothermal route. Figure 9 shows the cycling curves obtained for this material used as positive electrode in sodium and lithium cells. Despite the real different particles and aggregates morphologies, the electrochemical cycling curves of sodium and lithium cells are close to the ones obtained for cells with $\text{Na}_3\text{Fe}_3(\text{PO}_4)_4$ prepared by solid-state reaction with no significant improvements in capacities and polarization. Nevertheless, the profile recorded for the lithium cell is sloppier than the one obtained for the sample prepared by solid-state reaction. Such modification of the voltage profile could be due to a significant change in the surface energy as studied by Van der Ven and Wagemaker.¹⁶

No clear improvements in the performances are observed, despite really different particle sizes in the direction perpendicular to the plate (50 nm for the “hydrothermal” sample vs 300 nm for the “solid-state” sample), which should correspond to the *a* parameter direction. We first thought that this was proof that the alkaline ion diffusion occurs mainly in the (*b,c*) plane, i.e., in the interslab space, and that the tunnels in the [110] and $[\bar{1}\bar{1}0]$ directions, as depicted in Figure 1(c), do not take part in the diffusion pathway. However, the coherence length calculated from Sherrer's formula for the phase prepared by hydrothermal reaction from the full width at half-maximum of the (200) diffraction line: 50 nm is pretty close to the one found from our full analysis of the XRD pattern of $\text{Na}_3\text{Fe}_3(\text{PO}_4)_4$ prepared by solid-state reaction, i.e., 87 nm.¹⁵ The sample prepared by the solid-state reaction should therefore be built up from thin sheets stacked along the *a* direction and does not exhibit a well crystalline structure all along the 300 nm of thickness. We, therefore, do not have any evidence for a preferential direction for the diffusion for the alkaline ions.

Tables

Table I. Fitted Mössbauer parameters of the spectra of $\text{Na}_3\text{Fe}_3(\text{PO}_4)_4$ and the Li cell electrodes at the end of the first discharge: $\text{Li}_{1.9}\text{Na}_3\text{Fe}_3(\text{PO}_4)_4$ and at the end of the first cycle back to $\text{Na}_3\text{Fe}_3(\text{PO}_4)_4$.

	δ (mm/s)	Δ (mm/s)	Γ (mm/s)	%	Site
$\text{Na}_3\text{Fe}_3(\text{PO}_4)_4$	0.409(5)	1.153(5)	0.294(4)	36(1)	$\text{Fe}^{3+}(1)[\text{O}_h]$
	0.413(3)	0.315(3)	0.336(3)	64(1)	$\text{Fe}^{3+}(2)[\text{O}_h]$
End of discharge $\text{Li}_{1.9}\text{Na}_3\text{Fe}_3(\text{PO}_4)_4$	0.42(2)	1.03(2)	0.31(2)	19(4)	$\text{Fe}^{3+}(1)[\text{O}_h]$
	0.42(2)	0.38(2)	0.38(1)	35(4)	$\text{Fe}^{3+}(2)[\text{O}_h]$
	1.18(5)	2.80(5)	0.27(2)	12(4)	$\text{Fe}^{2+}(1)[\text{O}_h]$
	1.08(5)	2.37(5)	0.58(3)	34(4)	$\text{Fe}^{2+}(2)[\text{O}_h]$
End of cycle $\text{Li}_x\text{Na}_3\text{Fe}_3(\text{PO}_4)_4$	0.400(6)	1.119(6)	0.275(5)	36(1)	$\text{Fe}^{3+}(1)[\text{O}_h]$
	0.411(4)	0.308(4)	0.303(4)	64(1)	$\text{Fe}^{3+}(2)[\text{O}_h]$

3.4. General discussion

In this general discussion, we aim to interpret the difference in behavior between sodium and lithium cells as $\text{Na}_3\text{Fe}_3(\text{PO}_4)_4$ is used as the positive electrode. As sodium ions are intercalated in the framework, a variation in the cell parameters were observed together with a preferential reduction of the Fe(2) ions.¹⁵ The extra Na^+ ions should therefore occupy positions nearby the Fe(2) ions that are closer to the interslab space, and Na(1) and Na(2) ions should participate in the accommodation of the extra ions by diffusing in the framework leading to a low polarization of the cell. On the opposite, the intercalation of Li^+ ions do not lead to significant variation in the cell parameters and Fe(1) and Fe(2) are equivalently reduced. We believe that the Li^+ ions are located in the cavity of the slab, seen in [Figure 1](#), close to both Fe(1) and Fe(2) sites what could lead to a shrinkage of the cavity, thus compensating the expansion of the Fe(1) and Fe(2) sites occupied by big Fe^{2+} ions. Moreover, in the Li^+ ions intercalation/deintercalation process, the Na^+ ions do not seem to participate. The smallest Li^+ ions would have to “find” a diffusion path to reach the cavities that can lead to a lower lithium ionic diffusion in the sample compared to the sodium case and therefore to a higher polarization of the cell.

4. Conclusion

$\text{Na}_3\text{Fe}_3(\text{PO}_4)_4$ prepared by a solid-state reaction was studied as a positive electrode in lithium batteries. Up to 1.9 Li^+ ions/f.u. could be intercalated and only 1.7 Li^+ ions could be extracted between 2 and 4.5 V vs Li^+/Li with an average voltage of around ~ 2.8 V. In situ and ex situ XRD data and Mössbauer spectroscopy measurements indicate that during the intercalation/deintercalation process, the framework is maintained and that the process is pretty reversible (some lithium ions remain in the structure at the end of the cycle). Based on these studies, we believe that only the Li^+ ions are deintercalated during the first charge. Hydrothermal method has been successfully applied to the synthesis of $\text{Na}_3\text{Fe}_3(\text{PO}_4)_4$ and leads to a significant particle size reduction. However, no clear improvements in the cycling performances were observed using this material as the positive electrode in sodium and lithium batteries.

Acknowledgments

The authors thank Cathy Denage, Philippe Dagault, and Jérémy Humez for their technical support and Laurence Croguennec for fruitful discussions. This work was supported by Région Aquitaine and Ministère Tunisien de l'enseignement supérieur et de la recherche.

Centre National de la Recherche Scientifique assisted in meeting the publication costs of this article.

References

- [1] J. B. G. A. Manthiram, *J. Power Sources*, 26, 403 (1989)
- [2] C. Masquelier, A. K. Padhi, K. S. Nanjundaswamy, and J. B. Goodenough, *J. Solid State Chem.*, 135, 228 (1998).
- [3] A. K. Padhi, K. S. Nanjundaswamy, and J. B. Goodenough, *J. Electrochem. Soc.*, 144, 1188 (1997)
- [4] J. Barker, R. K. B. Gover, P. Burns, and A. Bryan, *Electrochem. Solid-State Lett.*, 8, A285 (2005).
- [5] A. Nyten, A. Abouimrane, M. Armand, T. Gustafsson, and J. O. Thomas, *Electrochem. Commun.*, 7, 156 (2005)
- [6] M. S. Kishore, V. Pralong, V. Caignaert, U. V. Varadaraju, and B. Raveau, *Electrochem. Commun.*, 8, 1558 (2006)
- [7] X. L. Ji, K. T. Lee, and L. F. Nazar, *Nature Mater.*, 8, 500 (2009)
- [8] J. Barker, M. Y. Saidi, and J. L. Swoyer, *J. Electrochem. Soc.*, 151, A1670 (2004)
- [9] B. L. Ellis, W. R. M. Makahnouk, Y. Makimura, K. Toghill, and L. F. Nazar, *Nature Mater.*, 6, 749 (2007)
- [10] N. Recham, J. -N. Chotard, L. Dupont, K. Djellab, M. Armand, and J. -M. Tarascon, *J. Electrochem. Soc.*, 156, A993 (2009).
- [11] T. J. Richardson, *J. Power Sources*, 119–121, 262 (2003)
- [12] B. Lajmi, M. Hidouri, M. Rzeigui, and M. Ben Amara, *Mater. Res. Bull.*, 37, 2407 (2002)
- [13] F. D'Yvoire, M. Pintardscrepel, and E. Bretey, *C. R. Seances Acad. Sci., Ser. C*, 290, 185 (1980)
- [14] K. H. Lii, *Eur. J. Solid State Inorg. Chem.*, 32, 917 (1995).

[15] K. Trad, D. Carlier, L. Croguennec, A. Wattiaux, B. Lajmi, M. Ben Amara, and C. Delmas, *J. Phys. Chem. C*, 114, 10034 (2010)

[16] A. Van der Ven and M. Wagemaker, *Electrochem. Commun.*, 11, 881 (2009).

Figures :

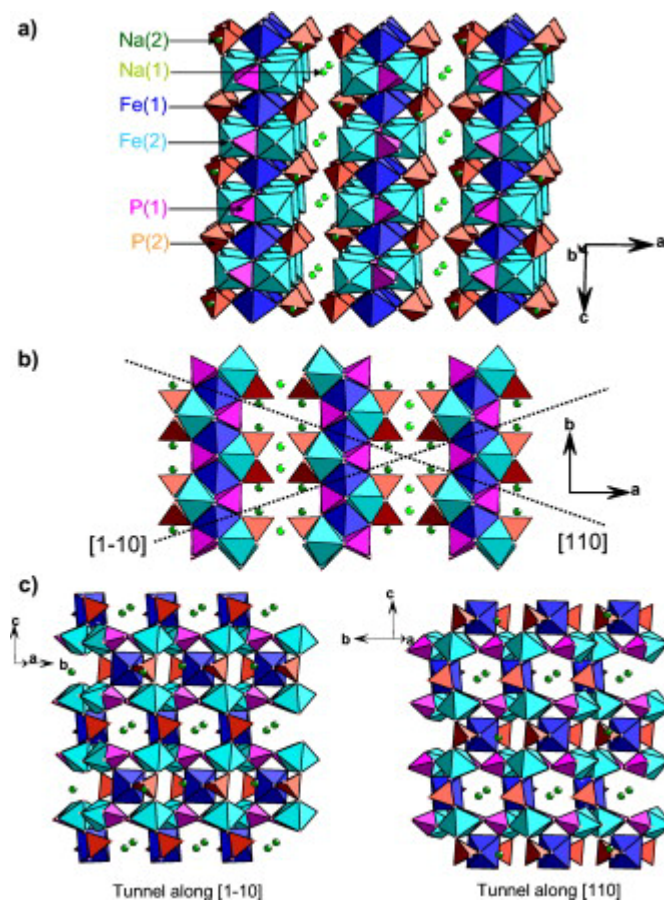


Fig. 1. (Color online) (a) View of the $\text{Na}_3\text{Fe}_3(\text{PO}_4)_4$ structure in the ac plane. (b) View of the $\text{Na}_3\text{Fe}_3(\text{PO}_4)_4$ structure in the ab plane. [(c) and (d)] Views of the $\text{Na}_3\text{Fe}_3(\text{PO}_4)_4$ structure respectively along $[110]$ and $[1\bar{1}0]$ directions showing tunnels.

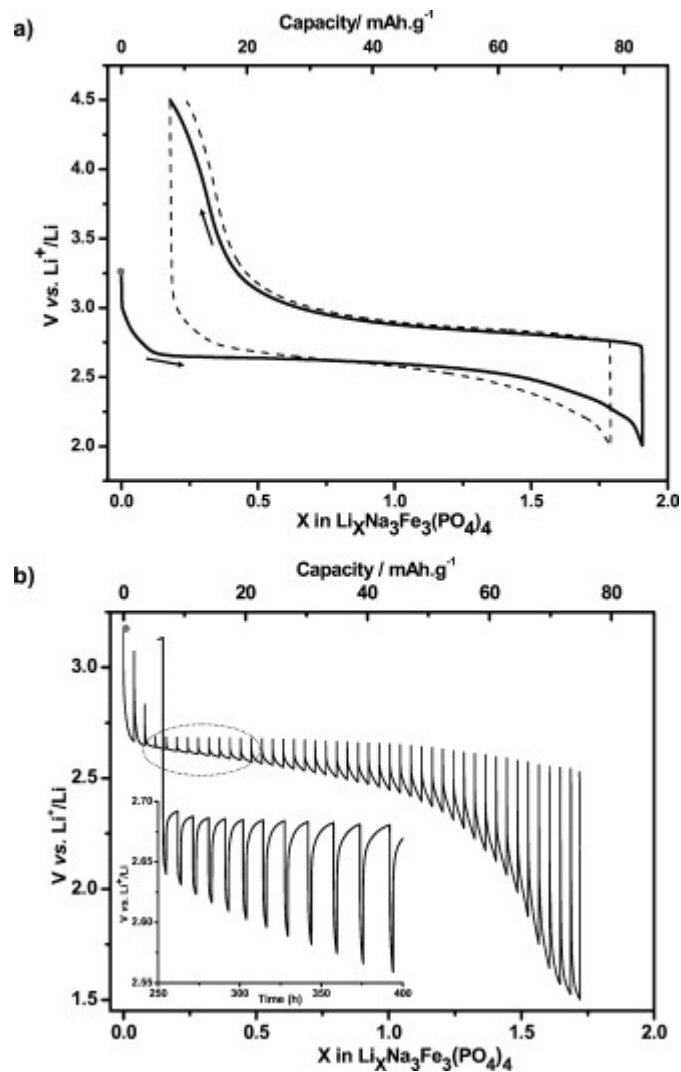


Fig. 2. Voltage vs intercalated lithium amount and capacity cycling curves obtained for a $\text{Li}^{\text{II}}\text{Na}_3\text{Fe}_3(\text{PO}_4)_4$ cell in the 4.5–2 V potential window with a C/100 cycling rate at room temperature. The red dot indicates the beginning of the cycling process. The second cycle is drawn with a dashed line. (b) OCV discharge profile of a $\text{Li}^{\text{II}}\text{Na}_3\text{Fe}_3(\text{PO}_4)_4$ cell with a C/100 rate. The evolution of the voltage vs time for a selected area is shown in the inset.

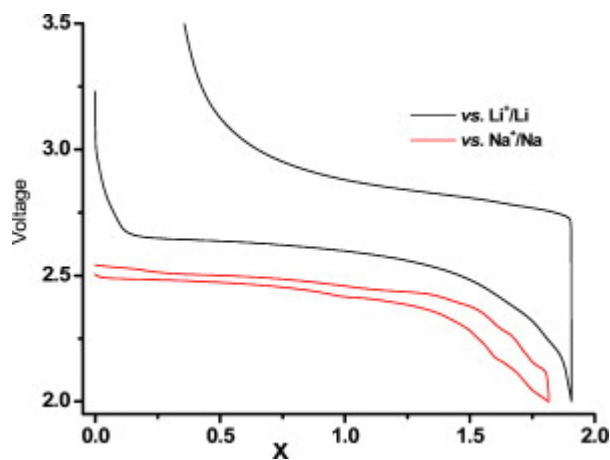


Fig. 3. (Color online) Comparison of the cycling curves of a $\text{Li}^{\text{II}}\text{Na}_3\text{Fe}_3(\text{PO}_4)_4$ cell (black line) and a $\text{Na}^{\text{II}}\text{Na}_3\text{Fe}_3(\text{PO}_4)_4$ cell (red line) both with a C/100 cycling rate at room temperature.

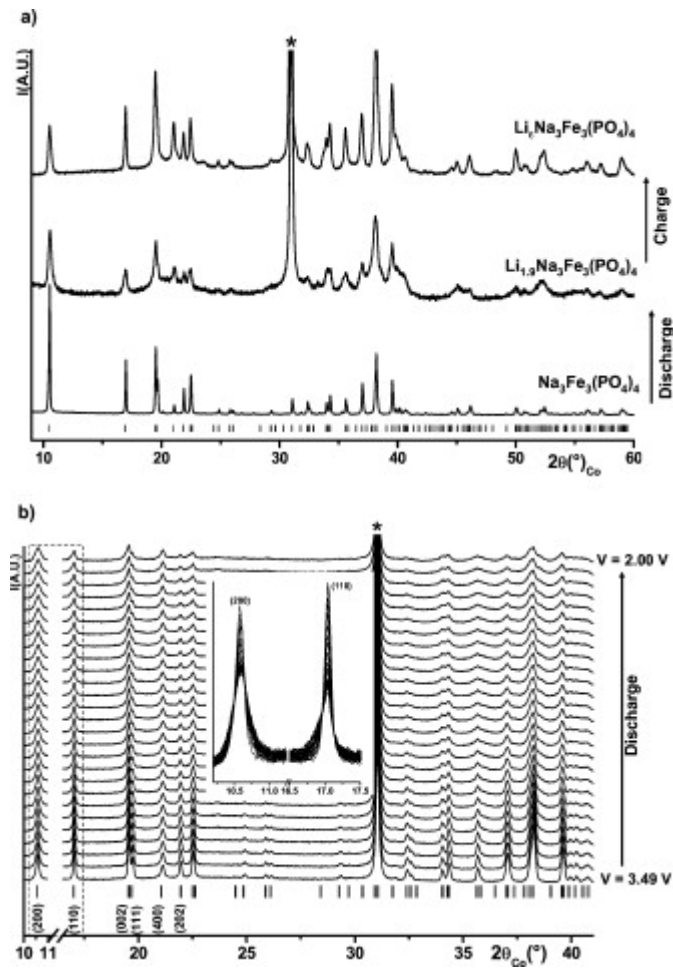


Fig. 4. (a) Ex situ XRD patterns of electrodes recovered at the end of the first discharge: $\text{Li}_{1.9}\text{Na}_3\text{Fe}_3(\text{PO}_4)_4$ and at the end of the first cycle: $\text{Li}_\infty\text{Na}_3\text{Fe}_3(\text{PO}_4)_4$ given in comparison with the XRD pattern of the initial $\text{Na}_3\text{Fe}_3(\text{PO}_4)_4$ phase. [(*) graphite diffraction peaks]. (b) In situ X-ray experiment during the first discharge of a $\text{Li}^{11}\text{Na}_3\text{Fe}_3(\text{PO}_4)_4$ cell. [(*) graphite diffraction peaks]

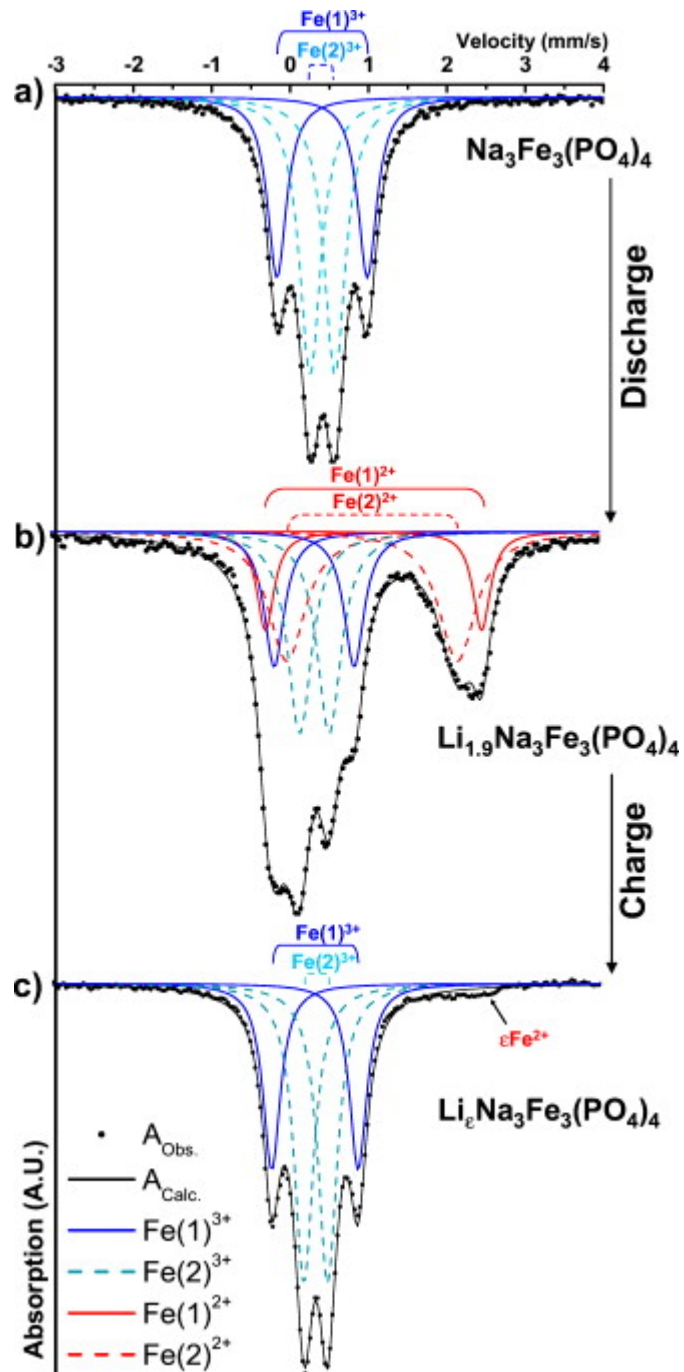


Fig. 5. (Color online) Mössbauer experimental and fitted spectra collected at room temperature on (a) $\text{Na}_3\text{Fe}_3(\text{PO}_4)_4$ and on electrodes recovered at the end of the first discharge: (b) $\text{Li}_{1.9}\text{Na}_3\text{Fe}_3(\text{PO}_4)_4$, and at the end of the first cycle: $\text{Li}_x\text{Na}_3\text{Fe}_3(\text{PO}_4)_4$ (c).

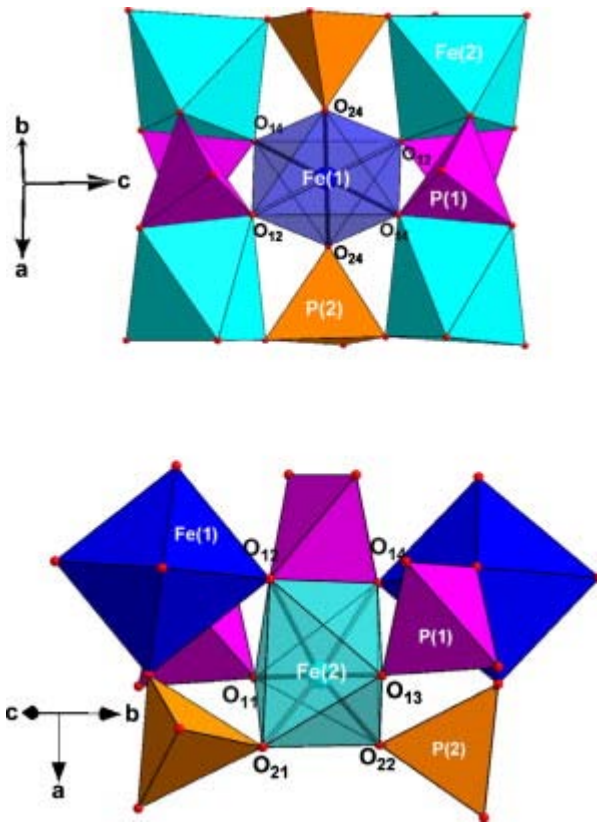


Fig. 6. (Color online) Local environments of Fe(1) and Fe(2) in $\text{Na}_3\text{Fe}_3(\text{PO}_4)_4$.

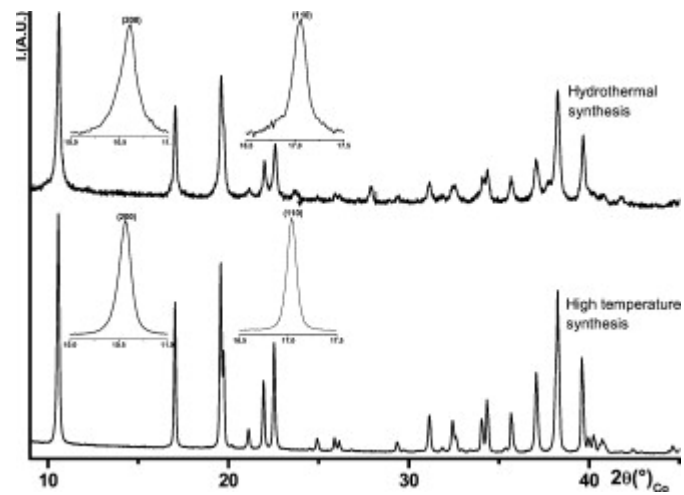


Fig. 7. XRD patterns of $\text{Na}_3\text{Fe}_3(\text{PO}_4)_4$ prepared by solid-state reaction and that prepared by hydrothermal reaction. The arrows indicate the presence of a small amount of $\text{Na}_3\text{Fe}_2(\text{PO}_4)_3$ as impurity.

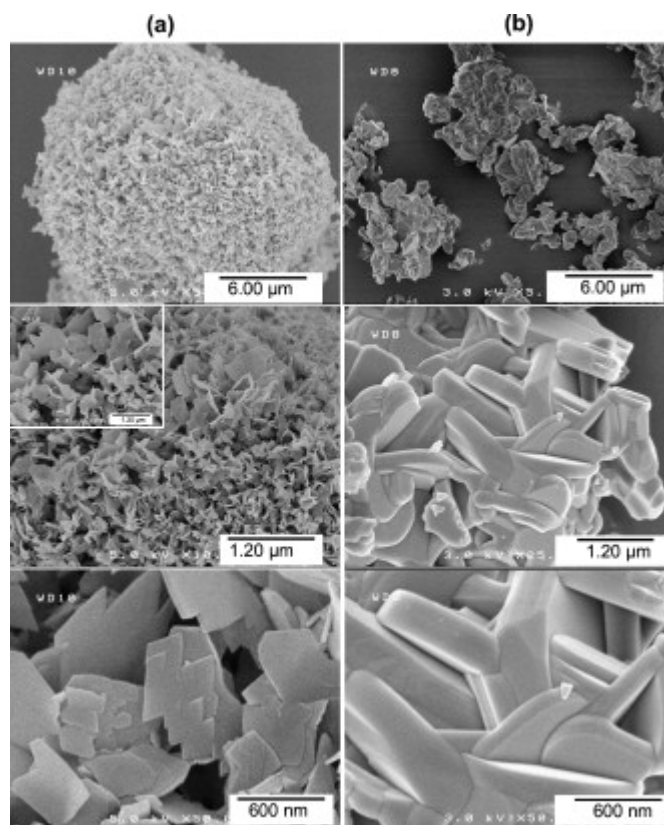


Fig. 8. SEM micrographs of $\text{Na}_3\text{Fe}_3(\text{PO}_4)_4$ powders (a) hydrothermally prepared at 200°C and (b) prepared at 750°C by solid-state reaction.

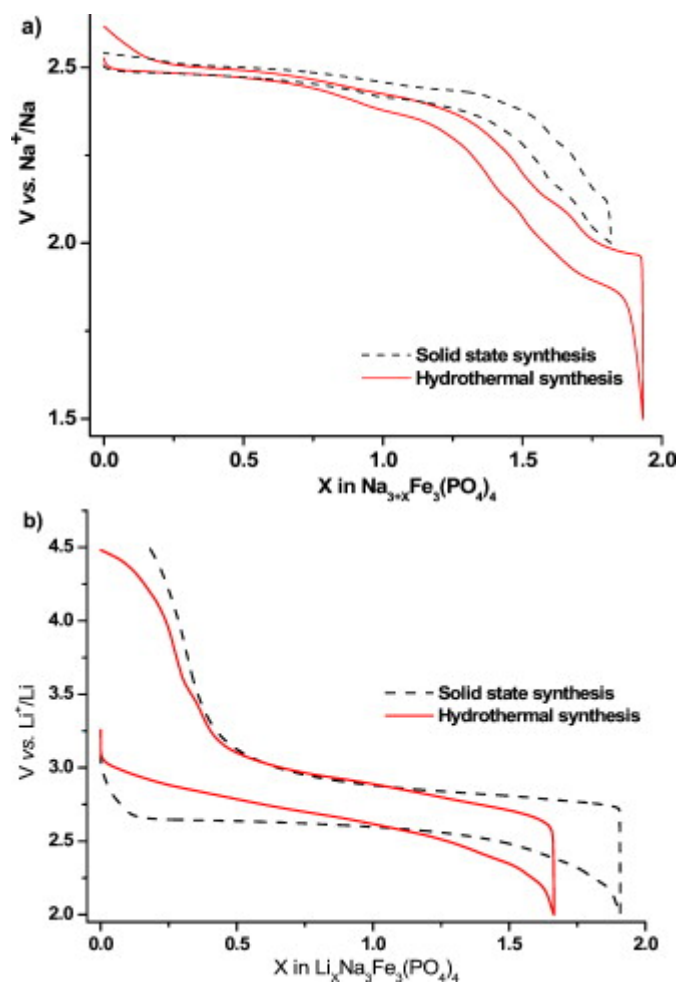


Fig. 9. (Color online) Electrochemical cycling curves of $\text{Na}_3\text{Fe}_3(\text{PO}_4)_4$ prepared by solid-state reaction (black line) and prepared by hydrothermal synthesis (red line) in Na (a) and Li (b) cells. (C/100 rate at room temperature).